

Intracranial Nonthermal Irreversible Electroporation: In Vivo Analysis

Paulo A. Garcia · John H. Rossmeisl Jr. · Robert E. Neal II · Thomas L. Ellis · John D. Olson · Natalia Henao-Guerrero · John Robertson · Rafael V. Davalos

Received: 6 January 2010 / Accepted: 22 June 2010 / Published online: 29 July 2010
© Springer Science+Business Media, LLC 2010

Abstract Nonthermal irreversible electroporation (NTIRE) is a new minimally invasive technique to treat cancer. It is unique because of its nonthermal mechanism of tumor ablation. Intracranial NTIRE procedures involve placing electrodes into the targeted area of the brain and delivering a series of short but intense electric pulses. The electric pulses induce irreversible structural changes in cell membranes, leading to cell death. We correlated NTIRE lesion volumes in normal brain tissue with electric field distributions from comprehensive numerical models. The electrical conductivity of brain tissue was extrapolated from the measured in vivo data and the numerical models. Using this, we present results on the electric field threshold necessary to induce NTIRE lesions (495–510 V/cm) in canine brain tissue using 90 50- μ s

pulses at 4 Hz. Furthermore, this preliminary study provides some of the necessary numerical tools for using NTIRE as a brain cancer treatment. We also computed the electrical conductivity of brain tissue from the in vivo data (0.12–0.30 S/m) and provide guidelines for treatment planning and execution. Knowledge of the dynamic electrical conductivity of the tissue and electric field that correlates to lesion volume is crucial to ensure predictable complete NTIRE treatment while minimizing damage to surrounding healthy tissue.

Keywords Brain cancer therapy · Minimally invasive surgery · Nonthermal ablation · Tumor ablation · Electroporation · Bioheat transfer · Finite element analysis · Electric field correlation · Electrical conductivity

P. A. Garcia · R. E. Neal II · R. V. Davalos (✉)
Bioelectromechanical Systems (BEMS) Laboratory, School of Biomedical Engineering and Sciences (SBES), Virginia Tech-Wake Forest University, Virginia Tech, 329 ICTAS Building, Stanger Street (MC 0298), Blacksburg, VA 24061, USA
e-mail: davalos@vt.edu

J. H. Rossmeisl Jr. · N. Henao-Guerrero · J. Robertson
Virginia–Maryland Regional College of Veterinary Medicine, Blacksburg, VA 24061, USA

T. L. Ellis
Department of Neurosurgery, Wake Forest University School of Medicine, Winston-Salem, NC 27157, USA

J. D. Olson
Center for Biomolecular Imaging, Wake Forest University School of Medicine, Winston-Salem, NC 27157, USA

R. V. Davalos
Bioelectromechanical Systems (BEMS) Laboratory, Department of Engineering Science and Mechanics (ESM), Virginia Polytechnic Institute and State University, Blacksburg, VA 24061, USA

Introduction

Nonthermal irreversible electroporation (NTIRE) is a promising new technique for the ablation of tissue and tumors (Davalos et al. 2005; Edd et al. 2006; Al-Sakere et al. 2007a, b; Rubinsky 2007). This minimally invasive procedure involves placing electrodes into or around a targeted area and delivering a series of short and intense electric pulses to induce irrecoverable structural changes in cell membranes, ultimately resulting in the death of the cell (Rubinsky et al. 2007). To achieve NTIRE, the electric field in the targeted region needs to be above a critical value, which is dependent on a variety of conditions such as tissue properties, electrode configuration and pulse parameters; including strength, shape, duration, number and repetition rate (Macek-Lebar and Miklavcic 2001; Davalos et al. 2005; Edd and Davalos 2007). However, for a specific tissue type and set of pulse conditions, the primary parameter

determining the extent of electroporation is the local electric field to which the tissue is exposed (Miklavcic et al. 2000). Davalos et al. (2005) demonstrated that NTIRE can be used to destroy substantial volumes of tissue *in vivo*. Following this, several researchers have confirmed the use of NTIRE in small and large animal models in the liver (Edd et al. 2006; Lee et al. 2007) and prostate (Onik et al. 2007), and in implanted mouse sarcomas (Al-Sakere et al. 2007a, b) using a variety of pulse parameters.

One advantage of NTIRE over other focal ablation techniques is the ability to destroy tissue through a non-thermal mechanism. As a result, it is possible at certain electric field intensities to kill the cells while preserving the extracellular matrix, axons, major blood vessels and other sensitive tissues, enhancing treatment outcome (Onik et al. 2007; Rubinsky 2007). The ablated volume can be predicted using numerical modeling for accurate treatment planning (Miklavcic et al. 2000; Pavselj et al. 2005). Researchers have shown that conductivity changes due to electroporation and joule heating can be incorporated in numerical models to produce more accurate predictions of treatment outcome (Davalos et al. 2004; Pavselj et al. 2005; Sel et al. 2005, 2007; Ivorra and Rubinsky 2007; Ivorra et al. 2009). Furthermore, the procedure can be monitored in real time using ultrasound and treatment outcome can be confirmed with ultrasound, CT and MRI (Lee et al. 2000, 2007; Garcia et al. 2009). Previous NTIRE studies outside the central nervous system (CNS) have shown that ablation is rapid in onset and resolution, allowing early repopulation of the ablated region with healthy cells (Onik et al. 2007; Rubinsky et al. 2007). Although treatment success is not dependent upon the immune system (Al-Sakere et al. 2007a, b), a tumor-specific immune response may be invoked (Onik et al. 2007).

Due to the aforementioned advantages, in conjunction with its short treatment time and minimally invasive nature, we hypothesize that NTIRE can be an effective brain cancer treatment. In order to allow for predictable and effective therapy, planning future brain cancer NTIRE treatments requires accurate knowledge of the electrical conductivity of the tissue and the electric field intensity needed for brain tissue ablation. In this study, we used numerical models to correlate a reconstructed NTIRE lesion volume in gray matter to an electric field distribution. Finite element software was used to develop a model capable of accounting for temperature and electroporation effects on brain tissue conductivity. This model was solved for the electric field distribution, which was used to correlate an electric field threshold for NTIRE lesions. Incorporating the conductivity dependence from electroporation and thermal effects provides a more accurate electric field–lesion correlation.

NTIRE lesions were generated within the ectosylvian gyral surface region of the brain in two canine subjects. The resulting lesion volumes were reconstructed from 0.2 and

7.0 T MRIs. These volumes were used with our revised numerical model to determine NTIRE electric field thresholds. In addition, the current and voltage data from the procedure were used to determine the bulk tissue baseline conductivity, σ_0 , of gray matter for NTIRE-relevant procedures. The electrical conductivity determines the electric field distribution, current and thermal effects from an NTIRE procedure. The results of this study can be used to improve treatment planning for patients using NTIRE for the ablation of brain tumors.

Materials and Methods

This pilot study was approved by the Institutional Animal Care and Use Committee and performed in a good laboratory practices–compliant facility at the Virginia–Maryland Regional College of Veterinary Medicine. Following the creation of a rostral tentorial craniectomy defect in two canine subjects, focal ablative NTIRE lesions were created in the cerebral cortex using the NanoKnife[®] generator (Angiodynamics, Queensbury, NY) with blunt tip probes (Ellis et al. 2010). The probes were 1 mm in diameter and surrounded by an insulating sheath, where 0.5-cm-long exposed tips were in contact with the tissue. These dimensions are smaller than the typical 1.27-mm-diameter commercial electrodes used in deep brain stimulation. Two probes (one energized and one set to ground) were used at a depth of 7 mm below the ectosylvian gyral surface, a noneloquent region of the brain. NTIRE lesions were created using the delivery criteria programmed into the NanoKnife[®], where nine sets of ten pulses at a frequency of 4 Hz were administered. Due to the recharging demands of the capacitors, the sets were separated by 1.0 s. The pulses were each 50 μ s in duration and were configured with alternating polarity between each set to minimize charge buildup on the electrode surface. The pulse parameters are given in Table 1. These pulses are in the lowest spectrum of the charge delivered to humans during electroconvulsive therapy, which typically varies between 0.5 and 512 mC (Jaffe 2002).

After administration of the NTIRE pulse train, intraoperative ultrasonography was used to assess the position and extent of the lesion created. Postoperatively, the canines underwent immediate MRI evaluation with and without contrast and then were recovered from anesthesia. Open source image analysis software (OsiriX, Geneva, Switzerland) was used to calculate the NTIRE focal ablation volumes. The lesions were traced in each of the 2-D postoperative MRI scans, and a solid 3-D representation of the NTIRE lesion volume was generated as in Garcia et al. (2009). A high-resolution (7.0 T) *ex vivo* MRI, which scans every 300 μ m, was also used for the second subject

Table 1 Pulse parameters used in NTIRE brain treatment of canine subjects

Subject	Electrode exposure (mm)	Separation distance (mm)	Voltage (V)	Volt-to-dist ratio (V/cm)	Total pulses	Pulse duration (μs)
1	5	5	1,000	2,000	9 × 10	50
2	5	5	500	1,000	9 × 10	50

in order to attain a more accurate NTIRE lesion reconstruction for the same NTIRE procedure.

Numerical modeling can be used to predict the electric field distribution and, thus, NTIRE treatment regions in tissue (Miklavcic et al. 2000; Pavselj et al. 2005; Edd et al. 2006). This has been chosen as the method to correlate lesion volume with an effective electric field threshold for NTIRE in brain. The methods for predicting NTIRE areas are similar to the ones described by Edd and Davalos (2007). The mathematical models were solved using a commercial finite element package (Comsol Multiphysics, v.3.5a; Stockholm, Sweden). The brain was modeled as a 7.0 × 5.0 × 5.0 cm ellipsoid with the electrodes inserted to a maximum depth of 0.7 cm. The electric field distribution is given by solving the Laplace equation:

$$\nabla \cdot (\sigma \nabla \varphi) = 0 \tag{1}$$

where σ is the electric conductivity of the tissue and φ is the potential. Because electrode placement resulted in the electrodes being surrounded mainly by gray matter, homogeneous physical properties were set to those of gray matter (Table 2). The electrodes were modeled as an insulating body with an extension of stainless steel. The electrical boundary condition along the tissue that is in contact with the energized electrode is $\varphi = V_0$. The electrical boundary condition at the interface of the other

electrode is $\varphi = 0$. The boundaries where the analyzed domain is not in contact with an electrode are treated as electrically insulative.

The numerical model incorporates the change in conductivity during a pulse resulting from the increased permeabilization to ions presumably associated with the creation of pores in the cell membrane (Ivorra 2010). Conductivity changes due to electroporation and temperature have been modeled to calculate the dynamic conductivity according to the following equation:

$$\sigma_{dynamic}(normE_{dc}, T) = \sigma_0 [1 + flc2hs(normE_{dc} - E_{delta}, E_{range}) + \alpha(T - T_0)] \tag{2}$$

where σ_0 is the baseline conductivity, α the temperature coefficient, T the temperature, and T_0 the physiological temperature (37°C). The *flc2hs* is a smoothed heavy-side function with a continuous second derivative that ensures convergence of the numerical solution. This function is defined in our numerical software (Multiphysics, v.3.5a), and it changes from 0 to 1 (over the range E_{range}) when $normE_{dc} - E_{delta} = 0$. In the function, $normE_{dc}$ is the magnitude of the electric field and E_{delta} is the magnitude of the electric field at which the transition occurs. In the simulations, we used $E_{delta} = 580$ V/cm and $E_{range} = \pm 120$ V/cm

Table 2 Physical properties used in the numerical simulations

Material	Quantity	Units	Value	Reference
Brain	α , Temperature coefficient	°C ⁻¹	0.032	(Duck 1990)
	k, Thermal conductivity	W m ⁻¹ K ⁻¹	0.565	(Duck 1990)
	c_p , Heat capacity	J kg ⁻¹ K ⁻¹	3,680	(Duck 1990)
	ρ , Density	kg m ⁻³	1,039	(Duck 1990)
	q''' , Metabolic heat generation	W m ⁻³	10,437	(Werner and Buse 1988)
Blood	c_b , Heat capacity	J kg ⁻¹ K ⁻¹	3,840	(Werner and Buse 1988)
	ρ_b , Density	kg m ⁻³	1,060	(Uzuka et al. 2001)
	w_b , Perfusion rate	s ⁻¹	7.15E-3	(Uzuka et al. 2001)
Insulation	σ , Electrical conductivity	S m ⁻¹	1.0E-5	(Cosman and Cosman 2005)
	k, Thermal conductivity	W m ⁻¹ K ⁻¹	0.01	(Cosman and Cosman 2005)
	c_p , Heat capacity	J kg ⁻¹ K ⁻¹	3,400	(Cosman and Cosman 2005)
	ρ , Density	kg m ⁻³	800	(Cosman and Cosman 2005)
Stainless Steel	σ , Electrical conductivity	S m ⁻¹	2.22E6	(Al-Sakere et al. 2007a, b)
Steel	k, Thermal conductivity	W m ⁻¹ K ⁻¹	15	(Cosman and Cosman 2005)
	c_p , Heat capacity	J kg ⁻¹ K ⁻¹	500	(Cosman and Cosman 2005)
	ρ , Density	kg m ⁻³	7,900	(Cosman and Cosman 2005)

in order to match the average brain tissue parameters used by others (Pavselj et al. 2005; Sel et al. 2005, 2007), where conductivity doubled due to electroporative effects between 460 and 700 V/cm. We assumed that once the conductivity increased due to electroporation it would not revert back. This process was repeated iteratively for each of the 90 pulses that were delivered in the experimental procedures. It should be noted that the thermal effect on conductivity was only taken into consideration when the electric field was below 460 V/cm since we assumed that the conductivity change due to electroporation already incorporates this dependence. Future research is needed to determine the brain tissue conductivity as a function of applied electric field and temperature changes for a more refined NTIRE treatment model.

To determine baseline conductivities for the two subjects used in this study, we matched the *in vivo* current measured by the NanoKnife® (resolution ± 0.2 A) during a typical pulse to the current of the numerically modeled NTIRE treatments. We used the current measured after the transient membrane charging effects had settled within the pulse. These conductivity values (Table 3) were determined by integrating the current density over the electrode surfaces and are within the expected ranges found in the literature (Latikka et al. 2001; Sel et al. 2007). The baseline conductivities were used with the dynamic conductivity function to simulate the complete 90-pulse NTIRE treatments.

Heating of the tissue resulting from the procedures was done by modifying the Pennes bioheat equation with the addition of a joule heating term $\sigma|\nabla\phi|^2$ (Davalos et al. 2003; Davalos and Rubinsky 2008). The modified equation is then

$$\nabla \cdot (k\nabla T) + \rho_b w_b c_b (T_a - T) + \dot{q}''' + \sigma|\nabla\phi|^2 = \rho c_p \frac{\partial T}{\partial t} \quad (3)$$

where k is the thermal conductivity of the tissue, T is the temperature, ρ_b is the blood density, w_b is the blood perfusion rate, c_b is the heat capacity of the blood, T_a is the arterial temperature, \dot{q}''' is the metabolic heat generation, ρ is the tissue density and c_p is the heat capacity of the tissue. The joule heating term was set to 0 when the pulses were off and only heat diffusion, perfusion and metabolic heat generation were involved in the heat transfer. Table 2 describes the physical parameters used in this study. The entire tissue is set to the initial physiological temperature

Table 3 Computed σ using *in vivo* intracranial NTIRE data

Subject	Voltage (V)	Current (A)	Total charge (mC)	σ_0 (S/m)
1	1,000	1.951 ± 0.2	9.89	0.30
2	500	0.361 ± 0.2	1.47	0.12

of the subjects measured prior to pulse administration: $T(x, y, z, 0) = 36.1$ and 36.8°C for the 500 and 1,000 V treatments, respectively. The electrode–tissue interface is set to continuity. The outer surface of the analyzed brain domain is mathematically considered to be thermally insulative and a proportional loss due to convective heat transfer, $h = 10 \text{ W}/(\text{m}^2 \text{ K})$, was set at the boundary of the electrodes exposed to air, as in Lackovic et al. (2009), with $T_\infty = 23^\circ\text{C}$. The initial temperature distribution of the brain and electrodes was allowed to reach equilibrium before the onset of the treatment to provide an accurate temperature distribution from the NTIRE pulses (Table 2) (Werner and Buse 1988; Duck 1990; Uzuka et al. 2001; Cosman and Cosman 2005; Al-Sakere et al. 2007a, b).

After modeling the entire treatment protocol with all aforementioned effects taken into account, the final electric field distribution at the end of the 90th pulse was used to correlate an electric field threshold with the experimental lesion volume. The volume of modeled tissue domain exposed to varying electric fields was integrated until the calculated volume was equal to the volume computed from the NTIRE lesion reconstruction.

In order to assess the thermal effects associated with the procedures, a “thermal isoeffective dose” analysis was used (Sapareto and Dewey 1984). Thermal isoeffective dose calculations are typically used for procedures involving complex variations in temperature as a function of time. Such calculations determine the amount of time it would take to equivalently damage the tissue as if it was held at a constant temperature. Although thermal damage can occur at lower temperatures for prolonged exposures, typically 43°C is chosen due to the abundant experimental data at this temperature (Sapareto and Dewey 1984; Dewhurst et al. 2003; Becker and Kuznetsov 2006). It has been shown that neuronal damage occurs if temperature is elevated to 43°C for 60 min ($t_{43} = 60$ min) (Matsumi et al. 1994). The following expression is the duration necessary to hold the tissue at 43°C to result in thermal isoeffective dose:

$$t_{43} = \int_{t=0}^{t=\text{final}} R^{(43-T_t)} dt \quad (4)$$

where T_t is the average temperature during the time interval dt , R is the number of minutes needed to compensate for a 1°C temperature change either above or below a breakpoint of 43°C and R is 0.25 when $T_t \leq 43^\circ\text{C}$ and 0.5 when $T_t > 43^\circ\text{C}$ (Sapareto and Dewey 1984; Matsumi et al. 1994). The thermal dose was integrated from the onset of pulses to 5 min after the conclusion of treatment, allowing heat dissipation to return the tissue to physiological temperature, thus incorporating all thermal effects from the procedure.

Results

Postoperatively, no adverse clinical effects were observed in the animals. The canine subjects did not demonstrate any adverse clinical effects after the procedure and were able to resume normal activities, such as eating, within 10 h of surgery. MRIs used to confirm the NTIRE lesion location and focality were performed within 60 min after completion of pulse delivery, and a high-resolution *ex vivo* scan is shown in Fig. 1. These 7.0 T MRIs were chosen since only the NTIRE lesion is visible and they include a superimposed schematic of the dual probes in order to guide the reader as to the placement of the electrodes.

From the *in vivo* MRIs, the acute intracranial lesions created with NTIRE procedures have classic MRI features of edema, inflammation and disruption of the blood–brain barrier (Thomas et al. 1996; Cherubini et al. 2005; Cha 2009). These MRI features have been correlated and confirmed with the presence of these pathological processes in postmortem pathological investigations, as previously reported (Garcia et al. 2009). Therefore, when measuring the treated area for the volume reconstructions, the hyperintense T2 W MRI scans were traced.

The 3-D reconstructed volumes corresponding to the NTIRE lesions from the treatments are shown in Fig. 2, where the dual probes were inserted perpendicular to the reconstructed lesion. The reconstructions of 1,000 and 500 V in Fig. 2 contain five and three white rings, respectively, corresponding to the number of traced slices. The varying voltages generated treatment areas that were approximately 10 (1,000) and 5 mm (500 V) along the major axis across the electrodes.

The computed baseline electrical conductivities, σ_0 , were found to be 0.30 and 0.12 S/m for the 1,000 and 500 V treatments, respectively (Table 3). These conductivity values are consistent with those typical in the literature

(Latikka et al. 2001; Sel et al. 2007) and were used to generate the electric field distributions. Figure 3 shows the conductivity map for the 1,000 V treatment after a 90-pulse NTIRE treatment, and it shows three main regions. The center area is the tissue that has been exposed to an electric field intensity greater than the threshold in our simulations (700 V/cm). There is also a transition region in which the conductivity varies between ~ 0.6 and ~ 0.3 S/m for electric field exposures between 460 and 700 V/cm. Finally, the regions that are below 460 V/cm only represent changes in conductivity due to thermal effects.

The electric fields found to correlate with the reconstructed lesion volumes in our experiments are shown in Table 4. For 90 50- μ s pulses delivered at 4 Hz it was found that 495 and 510 V/cm were the NTIRE thresholds for the 500 and 1,000 V experimental subjects, respectively. The electric field distributions for these thresholds at completion of the modeled treatment pulse application are shown in Fig. 4 in three Cartesian planes. The superimposed electric field isosurface plots represent the NTIRE-treated areas with 500 V (dark gray) and 1,000 V (light gray), respectively. One thing to note is that the dimensions of the NTIRE lesion are clearer in the x - y and x - z planes (Fig. 4a, c) compared to the y - z plane (Fig. 4b). In addition, the modeled lesion from 1,000 V extends several millimeters beyond the margin of the lower voltage treatment.

Figure 5 shows the temperature and thermal dose distributions generated during the NTIRE treatment of subject 1, which received the highest voltage used in the study. The maximum t_{43} values were calculated around the electrode–tissue interface, where the highest electric field intensity is generated, and thus, the greatest thermal effects due to joule heating from pulse administration. A maximum thermal isoeffective dose, t_{43} , of 40 min was calculated for subject 1, which was only in a small fraction of the treated tissue. This dose is insufficient to generate significant

Fig. 1 *Ex vivo* high-resolution 7.0 T MRI of NTIRE-treated brain in the second subject (500 V at an electrode separation of 5 mm). The exposed portions of the electrodes are depicted in *black* and their insulation in *white* to represent electrode placement

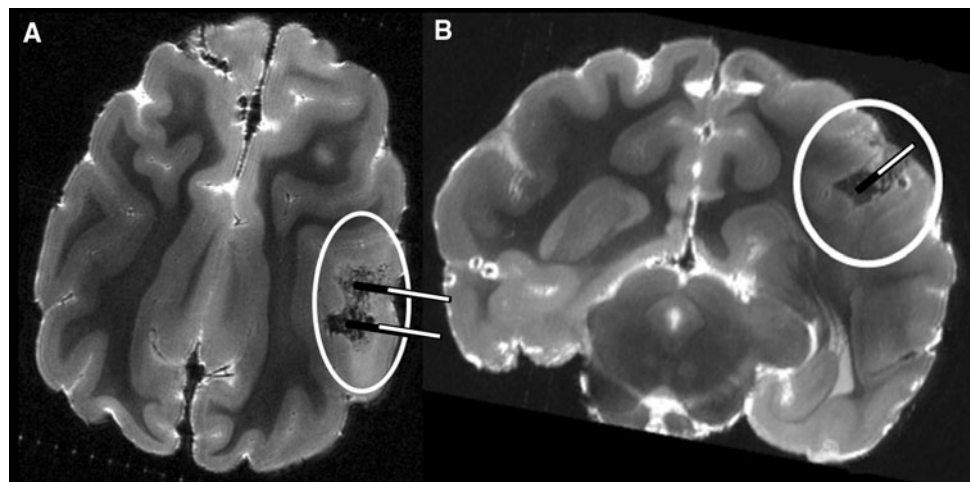


Fig. 2 MRIs (0.2 T) and 3-D reconstructions of the lesions in the canine brains showing in vivo axial slices for subjects treated with **a** 1,000 V (first subject) and **b** 500 V (second subject). The sets of slices from these MRIs were used to create the 3-D reconstructions of the lesions for the subjects treated with **c** 1,000 V and **d** 500 V. *White rings* correspond to the boundary between the area of lesion and normal brain from the postoperative 0.2 T axial MRI (figure not to scale)

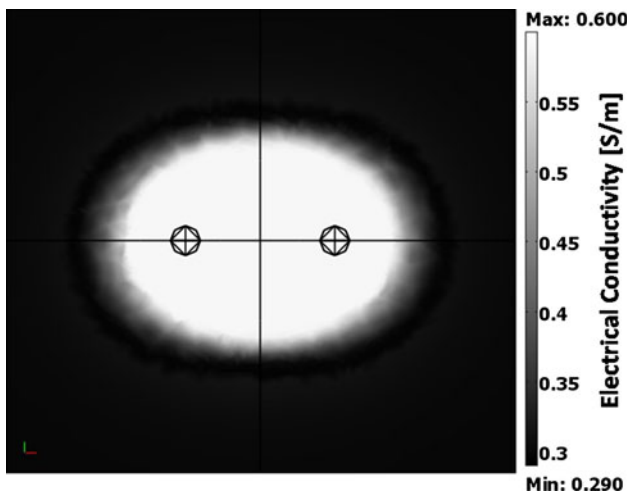
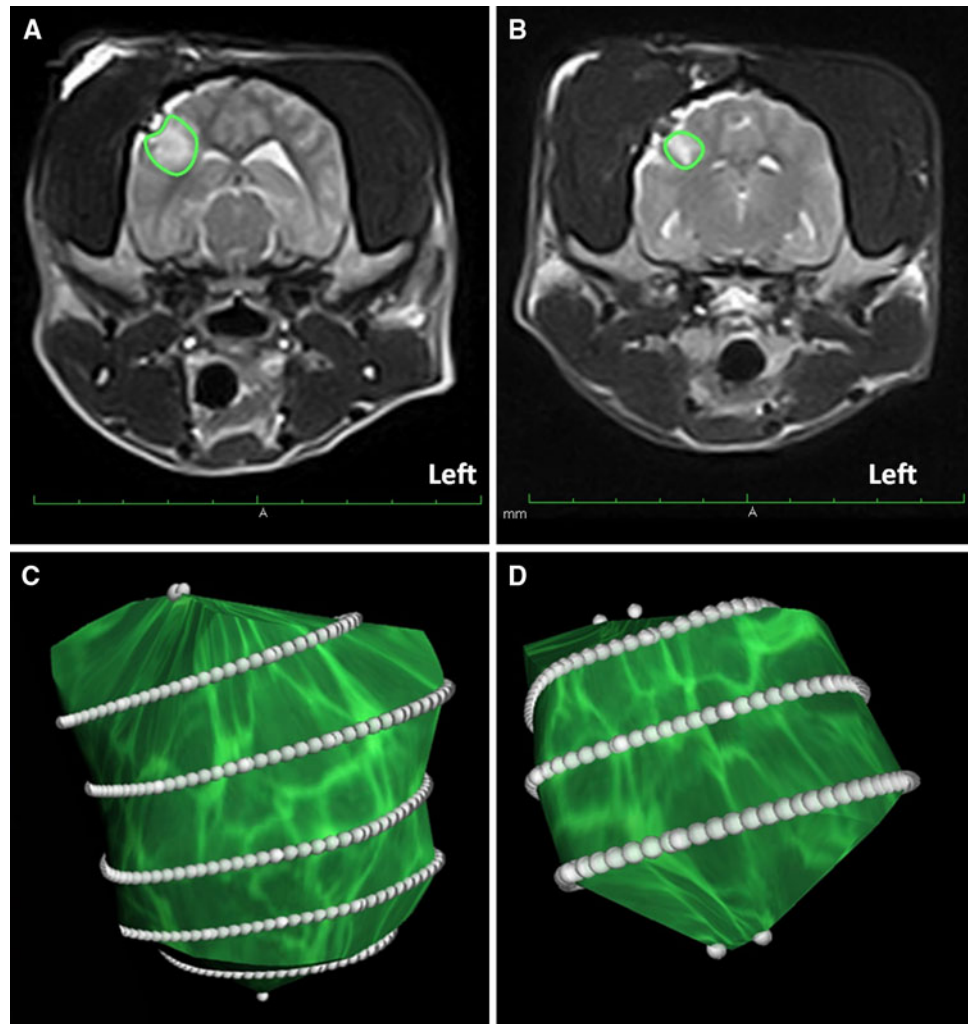


Fig. 3 Planar conductivity map of the tissue on the plane along the midline of the electrodes as a function of electric field and temperature. Conductivity is seen to be the highest near the electrodes and decreases as it moves farther away for parameters used in Subject 1 (Table 1)

Table 4 Computed lesion volume with corresponding electric field correlation

Subject	Voltage (V)	Volume (cm ³)	Electric field correlation (V/cm)
1–0.2 T MRI	1,000	0.599	510
2–0.2 T MRI	500	0.258	495
2–7.0 T MRI	500	0.250	501

neuronal thermal damage (Matsumi et al. 1994). These results indicate that thermal effects did not play a significant role in the ablation of canine brain tissue.

Discussion

We describe the electric conductivities, lesion volumes and electric field thresholds from the first systematic in vivo

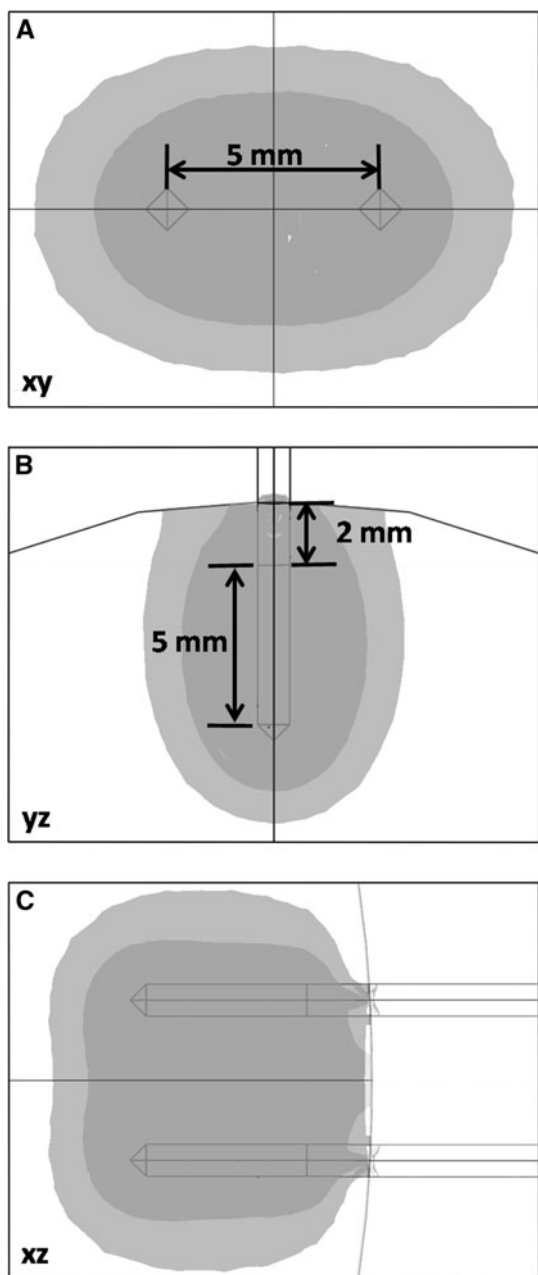


Fig. 4 Numerically modeled electric field results showing the lesion threshold outputs for the 500 V (dark gray) and 1,000 V (light gray) applied voltages. These volumes match the reconstructed lesions in Fig. 2

study of NTIRE for intracranial surgery (Ellis et al. 2010). Focal lesions were created in the right parietotemporal lobe of canine subjects using small, blunt-tip probes to minimize damage during insertion. The advantages of NTIRE include its ability to achieve ablation nonthermally compared to the mechanisms involved in cryoablation or radio frequency lesioning. This presents advantages over thermal focal ablation techniques because of its ability to spare major vasculature and the theoretical enhanced facilitation

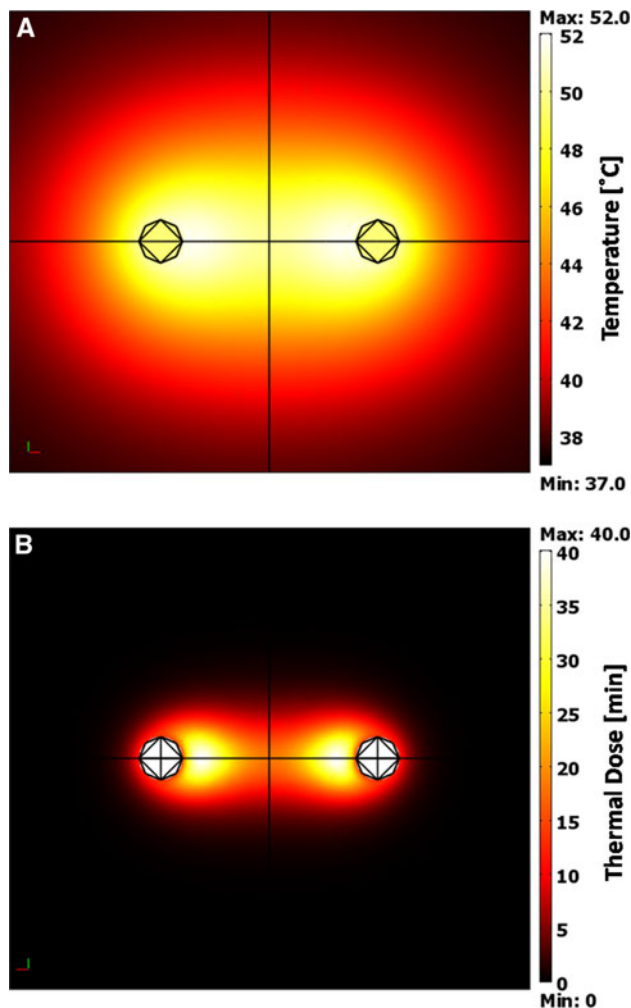


Fig. 5 **a** Planar map of the temperature distribution at the end of the final (ninetieth) electric pulse. **b** Cumulative I_{43} thermal dose equivalent 5 min after completion of the final electric pulse for 1000 V applied across electrodes 5 mm apart (Subject 1)

of drug delivery in reversibly electroporated regions of tissue (Davalos et al. 2005). Treatment application can be readily adapted for use with existing surgical and stereotactic guidance systems and technologies, and performed rapidly and minimally invasively. Furthermore, NTIRE has demonstrated vascular sparing effects and can be monitored in real time using ultrasound, CT or MRI. Current limitations of the technology appear to be primarily related to protocols with complex electrode design and placement logistics for ablating complex geometries, as well as treatment planning obstacles.

This study presents some of the important properties and responses of brain tissue undergoing NTIRE therapeutic electric pulses, with strong implications for treatment planning. The lesion volume reconstructions show affected regions of 0.258 and 0.599 cm³ for the protocol used with applied voltages of 500 and 1,000 V, respectively. When

these volumes were calibrated to numerical models that incorporate conductivity changes due to electroporation and temperature changes, it was found that an effective NTIRE electric field threshold of ~ 500 V/cm may be used to predict NTIRE ablation volumes in brain tissue using 90 50- μ s pulses delivered at a frequency of 4 Hz. It is important to note that when applying this threshold to lesion prediction during treatment planning, the numerical simulation should also incorporate the conductivity changes addressed in this model for the protocol being used to ensure accurate pairing with the calibrated NTIRE threshold.

In order to accurately predict the electric field distribution of an NTIRE procedure, the bulk conductivity and its changes due to electroporation and temperature play a major role. For the two protocols investigated, the current during a typical pulse was 0.361 ± 0.2 and 1.95 ± 0.2 A for applied voltages of 500 and 1,000 V, respectively, corresponding to baseline modeled bulk conductivities of 0.12 and 0.30 S/m. The difference between these baseline conductivities results from the nonlinear electric field dependence on conductivity that occurs due to tissue electrical changes during electroporation (Davalos and Rubinsky 2004; Lackovic et al. 2009).

It is important to note that the volumes of the lesions were reconstructed from MRIs taken within 60 min after pulse administration, so the observed ablation volume is likely to be that resulting from immediate NTIRE-induced cellular necrosis. This means that any additional cellular death resulting from late-onset apoptosis may not be taken into account in the electric field correlation. However, we have extensive pathological, immunohistochemical and ultrastructural data obtained 72 h postintracranial NTIRE from three canine subjects (data not shown) which clearly demonstrate that by this time point necrotic cell death is present. Furthermore, no significant differences in immunoreactivity to bcl-2, caspase-3 or caspase-9 were observed relative to untreated control brain tissue. These data suggest that the primary mechanism for cell death in these brain lesions was necrosis, and that later-onset apoptotic regions should not significantly alter the lesion volumes measured immediately after treatment.

Our studies have confirmed that in the brain the ablated volume is usually underestimated by MRI scans because of the coincidence of transient, NTIRE-induced perilesional vasogenic brain edema resulting from disruption of the blood–brain barrier. We have examined this with serial MRI examinations in canine subjects and confirmed it with pathological studies.

For reconstruction, the accuracy of the volumes was limited to the interval between the MRI scans (2.5 mm). Therefore, the high-resolution (7.0 T) scans of the ex vivo brain from subject 2, which used 300- μ m slices, may provide

a better representation of the lesion and were thus used for matching the NTIRE threshold. The high-resolution ex vivo 7.0 T MRI from the second subject resulted in a measured volume of 0.25 cm³. This corresponds to an electric field intensity of 501 V/cm, which is similar to that found from the 0.2 T MRI reconstructions. However, this lesion may be limited in accuracy due to shrinkage from fixation.

To the best of our knowledge, our NTIRE investigations in the brain are the first to use NTIRE pulse durations that are 50 μ s. This is considerably shorter than those described in previous studies (100 μ s–20 ms) (Edd et al. 2006; Al-Sakere et al. 2007a, b; Lee et al. 2007; Onik et al. 2007). It should be noted that the degree of electroporation is dependent on a variety of conditions such as tissue type, cell size and pulse parameters; including pulse shape, duration, number and repetition rate (Macek-Lebar and Miklavcic 2001; Mir 2001). The shorter pulse durations allow for a reduced charge delivered to the tissue and minimize the heating generated by the procedure. This reduction in heating allows for larger voltages to be used, and thus larger lesions, while retaining the positive characteristics associated with NTIRE therapy. Alternatively, smaller and more targeted lesions can be achieved by decreasing the voltages between the NTIRE treatments. Doing so in combination with customized electrode geometries and pulse parameters should allow for precise ablation of volumes with varying sizes and shapes.

The temperature generated by the electric pulses was calculated, and it was confirmed that the energy generated by the procedures was insufficient to induce thermal damage, even at the regions experiencing the greatest thermal effects, reinforcing the notion that NTIRE is an independent tissue ablation modality. Since thermal damage is a function of temperature and length of exposure, the negligible thermal damage associated with this procedure can be explained by the fact that an electroporation pulse is typically a fraction of a second in duration (Al-Sakere et al. 2007a, b; Edd et al. 2006). Furthermore, pulses were delivered at a frequency of 4 Hz, which is significantly faster than current typical procedures using ECG synchronization rates to avoid cardiac arrhythmias (Ball et al. 2010; Thomson 2010). Slowing the repetition rate with ECG synchronization will allow more time for heat dissipation by the vasculature, further reducing thermal effects. It should be noted that thermal dose analysis is generally used for long-term exposures of tissues to elevated temperatures. Therefore, the analysis used may not be ideal for electroporation investigations due to the burst of energy during the pulses. Nevertheless, it provides insight into the assessment of thermal damage in the regions of highest electric field.

An important limitation to the accuracy of this study is the relatively sparse amount of literature related to the conductivity of brain tissue and the inherent changes

resulting from electroporation. Although the change in conductivity due to electroporation values was taken from previous investigations (Sel et al. 2007), these data were based on hypothetical values that corresponded to known thresholds for rabbit liver tissue (Sel et al. 2005). Therefore, they do not fully account for the thermally dependent conductivity changes that occur due to cumulative joule heating associated with complete NTIRE treatment. Despite this, it was found that varying the degree of thermal changes in conductivity did not significantly alter the correlated NTIRE electric field threshold. However, in order to develop a greater understanding of these phenomena, future studies on the brain should experimentally measure the changes in temperature and conductivity of the tissue due to NTIRE.

In order to obtain an even greater degree of accuracy when correlating lesion volumes with numerically modeled electric fields, future modeling studies should incorporate tissue heterogeneities in order to understand their influence on the resulting electric field and temperature distributions. It has been previously shown that the heterogeneous relations between different tissue types, such as gray vs. white matter brain tissue, play a significant role in the electric field distribution, and thus in the NTIRE ablation zone (Neal and Davalos 2009). Knowledge of the heterogeneous properties of these tissues may improve the outcome of an NTIRE procedure by allowing for planning of electric field distributions that will enhance tissue selectivity. In addition, these studies would allow even more precise correlation between numerically modeled volumes and those seen on postprocedure MRI. This will be necessary in order to develop image-based treatment planning algorithms and the software necessary for their implementation.

This study presented a method of computing the baseline electric conductivity based on measured current during a typical pulse and numerical methods. To keep experimental invasiveness low, the conductivity was backed out from the current measured by the pulse generator. More precise current readings would help to provide a more accurate initial conductivity. However, because the NTIRE electric field distribution is determined by the conductivity map rather than the absolute conductivity (which will change with the baseline), this should not greatly affect the thresholds determined here. Previous electroporation investigations in other tissues have reported significant increases in conductivity during pulses compared to when the pulses are off. The conductivity increase is higher during the pulse, presumably due to the contributions of short- and long-lived pores (Ivorra 2010). However, in our typical pulses we did not observe this phenomenon, likely due to the limitations of the equipment. In order to allow for more accurate treatment planning and outcome prediction, the dependence of the electrical conductivity on

individual subjects and treatment location should be monitored before, during and after an NTIRE procedure using similar methods to the ones proposed by Cukjati et al. (2007). By comparing the behavior of conductivity during pulse application with that predicted by numerical models, one may monitor treatment progress and prevent damage beyond the volume of intended ablation. Furthermore, conductivity measurements could be taken immediately prior to pulse administration using a low-strength pulse, insufficient to induce electroporation, which would be applied in finalizing treatment planning.

Conclusion

This study examined the effects of NTIRE on brain tissue *in vivo* and used them to derive some of the properties and behaviors of brain tissue essential for effective treatment planning. Techniques were developed to use voltage and current data during a typical pulse to determine appropriate bulk baseline conductivities to be used in numerical simulations. Postoperative MRI scans were used to create 3-D lesion reconstructions for two treatment protocols. Numerical models incorporating conductivity changes as a function of electroporation and temperature were used to coordinate the lesion reconstructions with an electric field threshold. The findings presented in this study may be used to aid in planning for the application of NTIRE therapies in the treatment of brain cancer and other neuropathological disorders.

Acknowledgement This work was supported in part by the Coulter Foundation. Davalos acknowledges support from NSF CBET-0933335 towards the modeling effort presented in the manuscript. The authors thank Gregory B. Daniel, Carolina Ricco, Dana Calicott, Barbara Kafka and Stephanie Milburn for their assistance in surgery and Lindsey Buracker and Chris Arena for their help in treatment planning.

References

- Al-Sakere B, Andre F, Bernat C, Connault E, Opolon P, Davalos RV, Rubinsky B, Mir LM (2007a) Tumor ablation with irreversible electroporation. *PLoS ONE* 11:e1135
- Al-Sakere B, Bernat C, Andre F, Connault E, Opolon P, Davalos RV, Mir LM (2007b) A study of the immunological response to tumor ablation with irreversible electroporation. *Technol Cancer Res Treat* 6:301–306
- Ball C, Thomson KR, Kavnaudias H (2010) Irreversible electroporation: a new challenge in “out of operating theater” anesthesia. *Anesth Analg* 110:1305–1309
- Becker SM, Kuznetsov AV (2006) Numerical modeling of *in vivo* plate electroporation thermal dose assessment. *J Biomech Eng* 128:76–84
- Cha S (2009) Neuroimaging in neuro-oncology. *Neurotherapeutics* 6:465–477

- Cherubini GB, Mantis P, Martinez TA, Lamb CR, Cappello R (2005) Utility of magnetic resonance imaging for distinguishing neoplastic from non-neoplastic brain lesions in dogs and cats. *Vet Radiol Ultrasound* 46:384–387
- Cosman ER Jr, Cosman ER Sr (2005) Electric and thermal field effects in tissue around radiofrequency electrodes. *Pain Med* 6:405–424
- Cukjati D, Batiuskaite D, Andre F, Miklavcic D, Mir LM (2007) Real time electroporation control for accurate and safe in vivo non-viral gene therapy. *Bioelectrochemistry* 70:501–507
- Davalos RV, Rubinsky B (2004) Electrical impedance tomography of cell viability in tissue with application to cryosurgery. *J Biomech Eng* 126:305–309
- Davalos RV, Rubinsky B (2008) Temperature considerations during irreversible electroporation. *Int J Heat Mass Transfer* 51:5617–5622
- Davalos RV, Rubinsky B, Mir LM (2003) Theoretical analysis of the thermal effects during in vivo tissue electroporation. *Bioelectrochemistry* 61:99–107
- Davalos RV, Otten DM, Mir LM, Rubinsky B (2004) Electrical impedance tomography for imaging tissue electroporation. *IEEE Trans Biomed Eng* 51:761–767
- Davalos RV, Mir LM, Rubinsky B (2005) Tissue ablation with irreversible electroporation. *Ann Biomed Eng* 33:223–231
- Dewhirst MW, Viglianti BL, Lora-Michiels M, Hanson M, Hoopes PJ (2003) Basic principles of thermal dosimetry and thermal thresholds for tissue damage from hyperthermia. *Int J Hyperthermia* 19:267–294
- Duck FA (1990) Physical properties of tissues: a comprehensive reference book. Academic Press, San Diego
- Edd JF, Davalos RV (2007) Mathematical modeling of irreversible electroporation for treatment planning. *Technol Cancer Res Treat* 6:275–286
- Edd JF, Horowitz L, Davalos RV, Mir LM, Rubinsky B (2006) In vivo results of a new focal tissue ablation technique: irreversible electroporation. *IEEE Trans Biomed Eng* 53:1409–1415
- Ellis TL, Garcia PA, Rossmeisl JH, Henao-Guerrero N, Robertson J, Davalos RV (2010) Nonthermal irreversible electroporation for intracranial surgical applications. *J Neurosurg* (in print)
- Garcia PA, Rossmeisl JH, Robertson J, Ellis TL, Davalos RV (2009) Pilot study of irreversible electroporation for intracranial surgery. *Conf Proc IEEE Eng Med Biol Soc* 1:6513–6516
- Ivorra A (2010) Tissue electroporation as a bioelectric phenomenon: basic concepts. In: Rubinsky B (ed) *Irreversible electroporation*. Springer, Berlin, pp 23–61
- Ivorra A, Rubinsky B (2007) In vivo electrical impedance measurements during and after electroporation of rat liver. *Bioelectrochemistry* 70:287–295
- Ivorra A, Al-Sakere B, Rubinsky B, Mir LM (2009) In vivo electrical conductivity measurements during and after tumor electroporation: conductivity changes reflect the treatment outcome. *Phys Med Biol* 54:5949–5963
- Jaffe R (2002) The practice of electroconvulsive therapy: recommendations for treatment, training, and privileging. A task force report of the American Psychiatric Association, 2nd edn. *Am J Psychiatry* 159:331
- Lackovic I, Magjarevic R, Miklavcic D (2009) Three-dimensional finite-element analysis of joule heating in electrochemotherapy and in vivo gene electrotransfer. *IEEE Trans Dielec Elec Insul* 16:1338–1347
- Latikka J, Kuurne T, Eskola H (2001) Conductivity of living intracranial tissues. *Phys Med Biol* 46:1611–1616
- Lee RC, Zhang D, Hannig J (2000) Biophysical injury mechanisms in electrical shock trauma. *Annu Rev Biomed Eng* 2:477–509
- Lee EW, Loh CT, Kee ST (2007) Imaging guided percutaneous irreversible electroporation: ultrasound and immunohistological correlation. *Technol Cancer Res Treat* 6:287–294
- Macek-Lebar A, Miklavcic D (2001) Cell electroporation to small molecules in vitro: control by pulse parameters. *Radiol Oncol* 35:193–202
- Matsumi N, Matsumoto K, Mishima N, Moriyama E, Furuta T, Nishimoto A, Taguchi K (1994) Thermal damage threshold of brain tissue—histological study of heated normal monkey brains. *Neurol Med Chir (Tokyo)* 34:209–215
- Miklavcic D, Semrov D, Mekid H, Mir LM (2000) A validated model of in vivo electric field distribution in tissues for electrochemotherapy and for DNA electrotransfer for gene therapy. *Biochim Biophys Acta* 1523:73–83
- Mir LM (2001) Therapeutic perspectives of in vivo cell electroporation. *Bioelectrochemistry* 53:1–10
- Neal RE II, Davalos RV (2009) The feasibility of irreversible electroporation for the treatment of breast cancer and other heterogeneous systems. *Ann Biomed Eng* 37:2615–2625
- Onik G, Mikus P, Rubinsky B (2007) Irreversible electroporation: implications for prostate ablation. *Technol Cancer Res Treat* 6:295–300
- Pavselj N, Bregar Z, Cukjati D, Batiuskaite D, Mir LM, Miklavcic D (2005) The course of tissue permeabilization studied on a mathematical model of a subcutaneous tumor in small animals. *IEEE Trans Biomed Eng* 52:1373–1381
- Rubinsky B (2007) Irreversible electroporation in medicine. *Technol Cancer Res Treat* 6:255–260
- Rubinsky B, Onik G, Mikus P (2007) Irreversible electroporation: a new ablation modality—clinical implications. *Technol Cancer Res Treat* 6:37–48
- Sapareto SA, Dewey WC (1984) Thermal dose determination in cancer therapy. *Int J Radiat Oncol Biol Phys* 10:787–800
- Sel D, Cukjati D, Batiuskaite D, Slivnik T, Mir LM, Miklavcic D (2005) Sequential finite element model of tissue electroporation. *IEEE Trans Biomed Eng* 52:816–827
- Sel D, Lebar AM, Miklavcic D (2007) Feasibility of employing model-based optimization of pulse amplitude and electrode distance for effective tumor electroporation. *IEEE Trans Biomed Eng* 54:773–781
- Thomas WB, Wheeler SJ, Kramer R, Kornegay JN (1996) Magnetic resonance imaging features of primary brain tumors in dogs. *Vet Radiol Ultrasound* 37:20–27
- Thomson K (2010) Human experience with irreversible electroporation. In: Rubinsky B (ed) *Irreversible electroporation*. Springer, Berlin, pp 249–254
- Uzuka T, Tanaka R, Takahashi H, Kakinuma K, Matsuda J, Kato K (2001) Planning of hyperthermic treatment for malignant glioma using computer simulation. *Int J Hyperthermia* 17:114–122
- Werner J, Buse M (1988) Temperature profiles with respect to inhomogeneity and geometry of the human body. *J Appl Physiol* 65:1110–1118